Yu She
Department of Mechanical and Aerospace Engineering,
The Ohio State University,
Columbus, OH 43210
e-mail: she.22@osu.edu

Hai-Jun Su[1]
Fellow ASME
Department of Mechanical and Aerospace Engineering,
The Ohio State University,
Columbus, OH 43210
e-mail: su.298@osu.edu

Deshan Meng
Department of Mechanical and Automation,
Shenzhen Graduate School,
Harbin Institute of Technology,
Guangdong, Shenzhen 518055, China
e-mail: dsmeng@hit.edu.cn

Siyang Song
Department of Mechanical and Aerospace Engineering,
The Ohio State University,
Columbus, OH 43210
e-mail: song.1252@osu.edu

Junmin Wang
Professor
Fellow ASME
Department of Mechanical and Aerospace Engineering,
The Ohio State University,
Columbus, OH 43210
e-mail: wang.1381@osu.edu

Design and Modeling of a Compliant Link for Inherently Safe Corobots

In this paper, we propose a variable width compliant link that is designed for optimal trade-off of safety and control performance for inherently safe corobots. Intentionally introducing compliance to mechanical design increases safety of corobots. Traditional approaches mostly focus on the joint compliance, while few of them study the link compliance. Here, we propose a novel method to design compliant robotic links with a safety constraint which is quantified by head injury criterion (HIC). The robotic links are modeled as two-dimensional beams with a variable width. Given a safety threshold, i.e., HIC constraint, the width distribution along the link is optimized to give a uniform distribution of HIC, which guarantees inherent safety for human operators. This solution is validated by a human–robot impact simulation program built in MATLAB. *A static model of the variable width link is derived and verified by finite element simulations. Not only stress in the link is reduced, this new design has a better control and dynamic performance quantified by a larger natural frequency and a larger bandwidth compared with designs made of uniform beams and compliant joints (CJs). The proposed variable width link takes full advantage of the link rigidity while keeps inherent safety during a human–robot impact. This paper demonstrates that the compliant link solution could be a promising alternative approach for addressing safety concerns of human–robot interactions.* [DOI: 10.1115/1.4038530]

1 Introduction

Corobots [1] are robotic devices that work in collaboration with human partners, which have already been used in variable environments: exoskeletons as human power amplifiers [2], haptic devices in virtual reality environments [3], rehabilitation [4,5], and so on. Unlike conventional robots which are kept completely separated from humans to ensure safety, corobots are designed to physically interact with humans in a shared workspace. Therefore, a premium consideration of corobots might be safety [6,7]. A robotic system cooperating with humans and sharing the same workspace should not injure people in normal operation, operational error, or mechanical failure [6].

To ensure robot safety in industrial environments, standards [8] regarding to risk assessment, safety-critical software, dynamic limits, emergency stops, and human–machine interface for corobots have been established. For traditional robots, these standards require full stop of the robot and cutting its power source. A new safety standard ISO-10218 [9] corobots, established in 2006, restricted the tool center point/flange velocity ≤ 0.25 m/s, dynamic power ≤ 80 W, and static force ≤ 150 N. The implementation of these standards is at the expenses of reduced performance and productivity.

To quantitatively measure injury severity, several standard indices from automotive and sports industries [10,11] have been developed. Gadd [12] proposed Gadd severity index which is calculated as integral of head acceleration in the whole duration of collision. Later this index has been refined to the well-known head injury criterion (HIC) [13]. A HIC value of 100 $m^{5/2} s^{-4}$ may be considered as a threshold for human–robot interaction [6]. Although HIC may be the most commonly used criterion to evaluate safety [14] on human–robot interaction, Gao and Wampler [15] and Haddadin et al. [16] raised doubts on HIC regarding to its appropriateness for the application of human–robot interaction. Impact force is another criterion used to evaluate the safety issue. Zheng and Hemami [17] derived a mathematical model to depict external impulsive forces acting on the robotic system. Haddadin et al. [16] considered the impact force may cause fractures of facial bones, and evaluated this criterion on the impact at typical robot velocities.

Solutions to address the safety concerns in industrial robots can be largely divided into two categories: sensor based and mechanical design based. The former approach relies on variable sensors including vision systems, proximity-sensitive skins, or torque/force sensor to detect collisions, followed by robust control algorithms. Once a collision is detected, active stiffness and impedance control are employed to introduce compliance in the joints. Howe and Cutkosky [18] studied tactile sensors placing on robot for detecting environment. Noncontact sensors, such as capacitance-based sensors, infrared sensors, and ultrasonic

[1]Corresponding author.

Manuscript received April 3, 2017; final manuscript received November 10, 2017; published online December 20, 2017. Assoc. Editor: K. H. Low.

sensors, were also studied to help the teleoperated robots to avoid collision [19,20]. Heinzmann and Zelinsky [21] studied computer vision based sensors to quantitatively ensure safety for physical human–robot interaction. Kong et al. [22] optimally designed the feedback and feedforward controllers to realize ideal force control for robots interacting with humans. Recently, artificial intelligence based on sensory system offered another methodology to address safety human–robot interaction. For instance, Najmaei and Kermani [23] use a class of artificial neural networks to obtain a superquadric-based model of human, which is used to evaluate the danger of robot operations. The sensor-based control of robots is one of the most promising methods to address the safety issues [24]. A coherent description of the sensorized environment could be obtained via fusion of data from those sensors, which can be addressed by artificial intelligence. The sensor-based approach addresses the safety issue at the cost of redundant sensors and complex fusion algorithms.

The second approach is mechanical design based. The compliant mechanical design typically absorbs kinetic energy during the impact duration, hence could reduce the impact energy transferred to humans. The mechanical compliance approach offers inherent safety, i.e., the safety is intrinsically guaranteed and not subject to malfunctioning of sensors. Typical representatives of the mechanical compliance include joint compliance and link compliance. Zinn et al. [25] designed a distributed macro-mini actuation (DM2) which employs a pair of two actuators for the shoulder and elbow joints, generating low and high frequency torque components, respectively. Bicchi et al. [7] designed compliant nonlinear actuators which equipped the robot system with intrinsic safety. Tonietti et al. [26] studied the transmission stiffness of the actuator from the viewpoint of mechanical and control. Bicchi et al. [27] investigated the mechanism and controller design of the actuator. Chen et al. [28] designed a clutch mechanism in parallel with its passive series elastic transmission element in the actuator to increase the safety of robot arms. Bicchi and Tonietti [6] designed actuator mechanisms with optimal control under safety constrains. Haddadin et al. [29] investigated the joint elasticity for inherent safety of a robot. Lim and Tanie [30] designed a robotic system with passive viscoelastic trunk and passively movable base, which secured human safety during unexpected collisions.

The mechanical design-based approach is by no means to replace the sensor-based approaches, but rather offers an alternative solution or complementary solution. The advantage of mechanical design approach is that safety is considered at the design stage rather than at run time.

Most compliant mechanical designs focus on the mechanical structure at the flexible joint with external parts on the robotics system, which increased extra mass, complexity, and costs of the robotic system. A few researches studied the variable compliant robotic links [31,32], but complex actuation is required for some case [33]. Therefore, we proposed a new solution which guaranteed the robot inherent safety without adding external materials and complexity on the robot meanwhile. The original concept was presented in Ref. [34]. In this paper, we present the compliant mechanical design and modeling, changing bending stiffness of the cross section of the manipulator for intrinsic safe robot design. Specifically, in this paper, the width of the manipulator was optimized with a safety constraint.

We begin this paper with an introduction of problem statement and safety criterion of impact in Sec. 2. Introducing mechanical compliance to a robot link is presented in Sec. 3. In Sec. 4, we develop the shape optimization framework for design of planar compliant links for inherently safe robots. In addition, the simulation of the human–robot interaction via Simmechanics is developed to verify the optimized solution. Static model is studied in Sec. 5, and performance evaluation of the optimized link with variable width is discussed in Sec. 6. Finally, conclusions and future work are presented in Sec. 7.

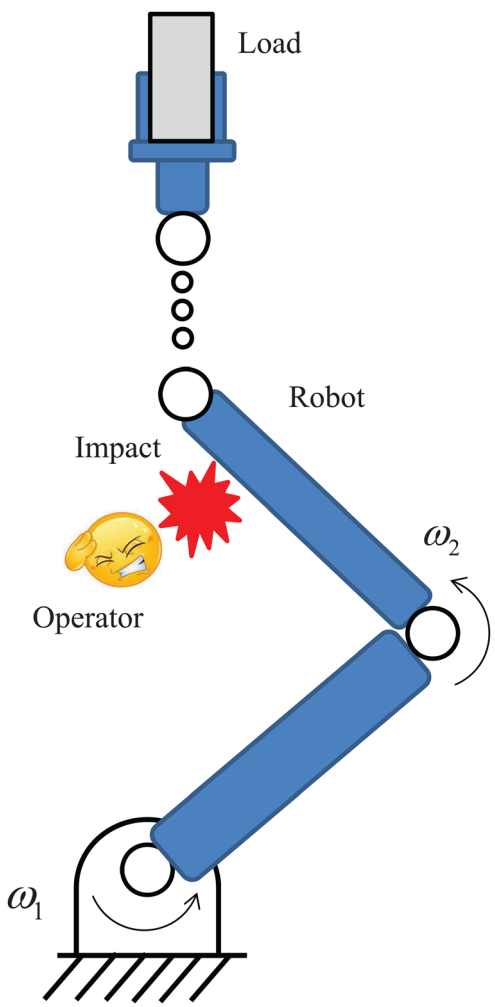

Fig. 1 Impact between the robot and the human operator occurs anywhere on the robotic links

2 The Problem Statement and Safety Criterion

Suppose an unexpected impact between a robot and an operator occurs, as shown in Fig. 1. The robot is comprised of a grasper

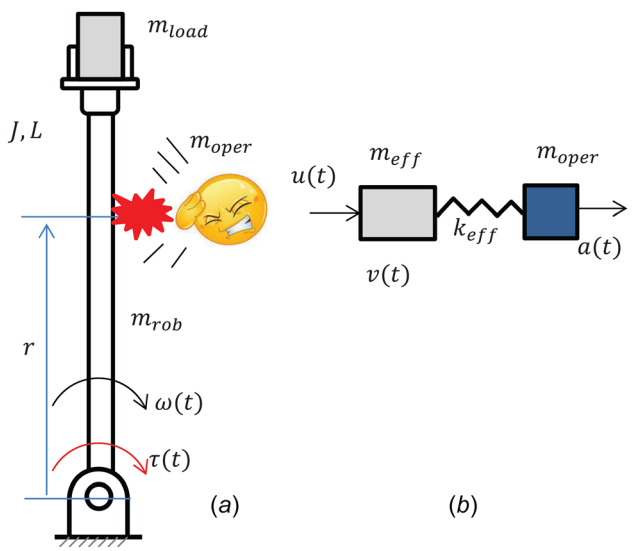

Fig. 2 A typical robotic link (*a*) and its mass–spring–mass impact model (*b*)

with load and one or more links, connected by joints. Since it shares workspace with human being, impact might occur at any position on the robot. Intuitively, the larger the distance between the impact position and the base, the higher the impact velocity, hence the more severe the injury.

Figure 2(*a*) shows a typical robotic link with a length L, with a mass m_{rob}, with a rotational inertia J, and with a load m_{load}. Driven by a torque controller $\tau(t)$, the operator's head with mass m_{oper} is hit by the link at the radius of r with an angular velocity $\omega(t)$.

Although there are some confusions and ambiguities of HIC in literatures [16], it still might be the most widely used criterion to evaluate severity of collision in a human–robot interaction. In this paper, the classical HIC index [10], was used to be a criteria to evaluate safety, then optimize the manipulator. The expression of HIC index is [15]

$$\text{HIC} = T\left[\frac{1}{T}\int_0^T \hat{a}\,dt\right]^{2.5} \tag{1}$$

where T is the time duration of impact, $\hat{a}(t)$ is the normalized head acceleration in gravity, i.e., $\hat{a} = a(t)/g$, where $a(t)$ is the actual acceleration of the head and g is the gravity acceleration [16]. The normalized head acceleration is given by $\hat{a} = A\sin\Omega t$, $0 \le t \le \pi/\Omega$, where Ω and A are radian frequency and magnitude of the normalized acceleration, respectively.

To compute HIC in terms of design parameters and impact velocity, a mass–spring–mass impact model, shown in Fig. 2(*b*) has been proposed in Ref. [6]. $v = \omega r$ is the initial impact velocity of the robotic link at the impact location, m_{eff} is the equivalent mass of the robot, and k_{eff} is the equivalent spring stiffness of the link and covering material of both the operator and robot. For a short impact period of the mass–spring–mass system, HIC index can be expressed as follows [6]:

$$\text{HIC} = 1.016T\left(k_{\text{eff}}^{0.75}\right)\left(\frac{m_{\text{oper}}^{-0.75}m_{\text{eff}}^{1.75}}{\left(m_{\text{eff}}+m_{\text{oper}}\right)^{1.75}}\right)\left(v^{2.5}\right) \tag{2}$$

Observing Eq. (2), it is observed that impact duration, effective stiffness, mass coefficients, and impact velocity are those factors affecting HIC value. Since we would like to optimize the arm while hold its performance, paying more attention to the effective stiffness is reasonable.

The mechanical model of the robot impact system can be described as shown in Fig. 3, where τ_m and ω_m are the motor's torque and angular velocity, respectively, and ω_r is the robot angular velocity. The effective stiffness could be affected by the joint stiffness between the motor and the link of k_j, the link stiffness of the link of k_l, and the stiffness of covering material of the operator of k_c. Since we study the case of compliant mechanisms, the stiffness of covering material is considered infinite larger and, its effect can be ignored in a serial connected spring system. Analysis and comparison of the effect of k_j and k_l are illustrated in Sec. 3.

3 Effect of Compliance on the Safety Criteria

In this section, different designs are compared in order to find the best one to be optimized. If effective stiffness k_{eff} is constant, HIC increases rapidly with regard to velocity, i.e., HIC $\propto v^{2.5}$. For traditional rigid link (RL) robots, k_{eff} is the stiffness of the covering materials, Fig. 4(*a*). To ensure safety, its speed must be significantly reduced. This is the main reason that it is very difficult to achieve a reasonable trade-off between performance and safety with velocity control only.

Let us consider methods for reducing the effective stiffness k_{eff}. Rather than only studying the worst case (impact at the free end), we would like to study HIC for any arbitrary impact position along the robotic link, defined by r, i.e., the impact velocity $v = r\omega$ where ω is the angular velocity of the link. We achieve this by intentionally introducing mechanical compliance into the design of robotic link. The easiest way to do so is to introduce compliance at the joint. Currently, there are several variable width joint/actuator designs in the literature [35]. These designs can be modeled as a rigid link with a torsion spring k_j at the joint, shown in Fig. 4(*b*). The effective stiffness of this design is $k_{\text{eff}} = k_j/r^2$. Substituting it into Eq. (2) yields HIC $\propto r$. This means that the HIC value is linearly distributed along the link starting from zero at the joint and maximum at the free end. As a comparison, this distribution is HIC $\propto r^{2.5}$ for the rigid link design. This result tells us that the introduction of compliant joint (CJ) smoothes out the HIC distribution throughout the link.

Now extending from the compliant joint design to the compliant link design, we consider a link with a uniform bending stiffness EI throughout the link, where E is the elastic modulus of the material, and I is the moment of inertia of the cross-sectional area. For the sake of generality, here we treat EI as a lumped parameter. Modeled as a cantilever link, the lateral stiffness of the compliant link at any impact position r is calculated as $k_{\text{eff}}(r) = 3\text{EI}/r^3$. Substituting it into Eq. (2) yields the distribution of HIC in terms of r as HIC $\propto r^{0.25}$. As shown in Fig. 4(*e*), the HIC of this design is a better approximation to a constant value than the other two designs.

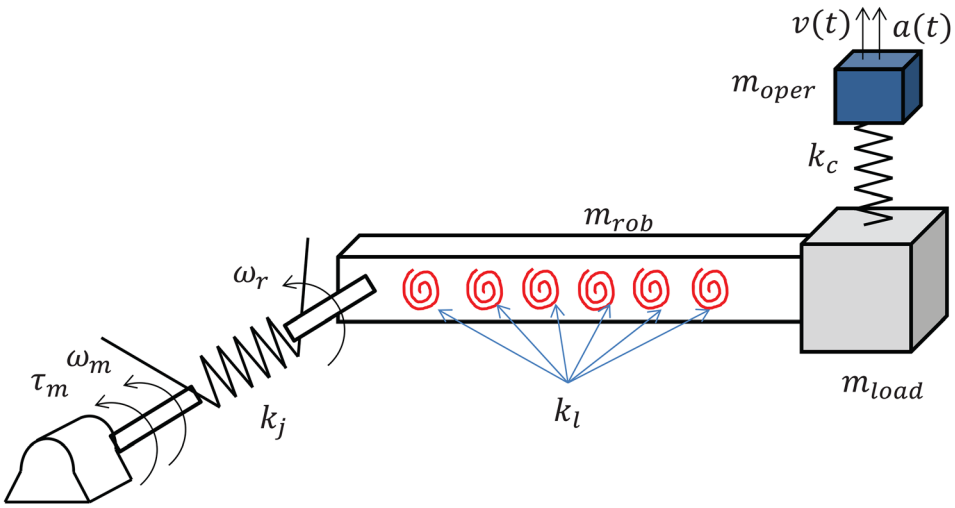

Fig. 3 The mechanical model of the robot impact system

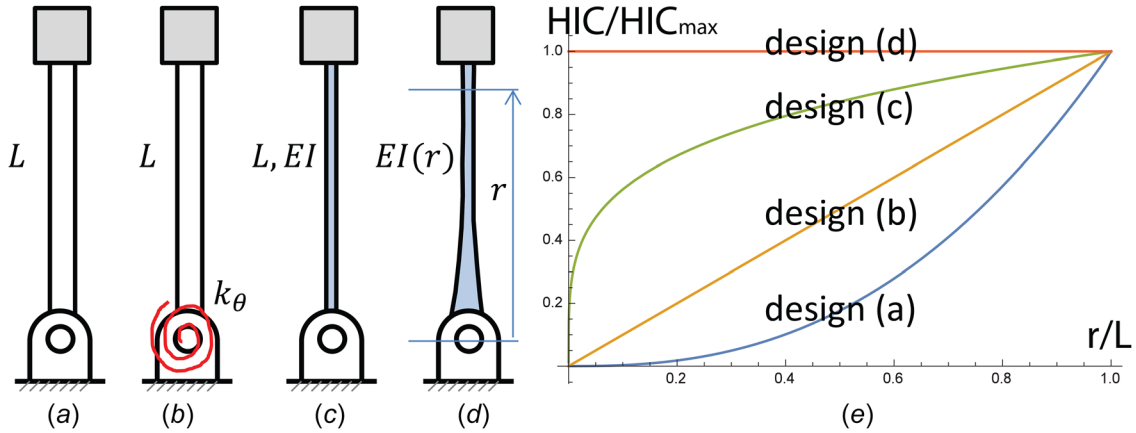

Fig. 4 Distribution of HIC versus impact position for several link designs: (*a*) a RL gives HIC $\propto r^{2.5}$, (*b*) a rigid link with a CJ gives HIC $\propto r$, (*c*) a flexible link with a uniform bending stiffness (*U*) results in HIC $\propto r^{0.25}$, and (*d*) a flexible link with variable bending stiffness (*V*) results in a constant HIC. (*e*) Comparison of HIC/HIC$_{max}$ for the four compliance designs.

The optimal solution of variable width link is obtained when HIC is constant throughout the entire link, Fig. 4(*d*). By examining Eq. (2), we can see that this occurs when $k_{\text{eff}}(r) \propto r^{-10/3}$. This means that if we can design or control the stiffness along the link according to this relationship, we can maximize the use of compliance for reducing the HIC level.

Based upon the above analysis, tentative case studies are conducted to explore the influence of bending stiffness on HIC distribution. A typical approach to change the bending stiffness is to change the width of the link. The variation of the width distribution of the link is given in Fig. 5, and we observe that the HIC distribution along the links are as shown in Fig. 6. As we can see from these tentative studies, it is possible to design a variable width link to achieve a uniform HIC distribution along the robot link for inherent safety, while maximal utilize mechanical compliance at the same time.

In Sec. 4 we will formulate this problem into a shape optimization problem. The design goal here is to determine the distribution of bending stiffness $EI(x)$ such that the HIC distribution is constant throughout the entire link.

4 Shape Optimization of Compliant Links for Safety Criteria

In this section, we seek to optimize a link with variable bending stiffness based upon a given HIC value. Given a maximum angular speed of the robotic link, the HIC value should be always below a safe threshold, which ensures that the robot is incapable of injuring people. In addition, the HIC value should be as close as possible to be a constant (the maximum HIC value) along the manipulator to better exploit the mechanical compliance. As discussed above, design of variable bending stiffness is able to satisfy this requirement.

4.1 Effective Stiffness of Links With a Variable Width. Suppose all variables except the effective stiffness k_{eff} in Eq. (2) are constant. Let us consider a rectangular link with a constant thickness t, a total length L, and a variable width $w(x)$ along the longitudinal direction. The effective lateral stiffness $k_{\text{eff}}(r)$ at any position r can be determined by F/δ, where F is a lateral force applied at $x = r$, and δ is the lateral deflection, as shown in Fig. 7(*a*). Mathematically, $k_{\text{eff}}(r)$ can be calculated as

$$k_{\text{eff}}(r) \equiv \frac{F}{\delta} = \frac{1}{\left[\int_0^r \frac{(x-r)^2}{EI(x)}dx\right]} = \frac{1}{\left[\int_0^r \frac{12(x-r)^2}{Etw(x)^3}dx\right]}, \quad 0 \le r \le L \tag{3}$$

For a given link width function $w(x)$, substituting Eq. (3) into Eq. (2) yields the HIC distribution along the longitudinal direction of the link, HIC(x).

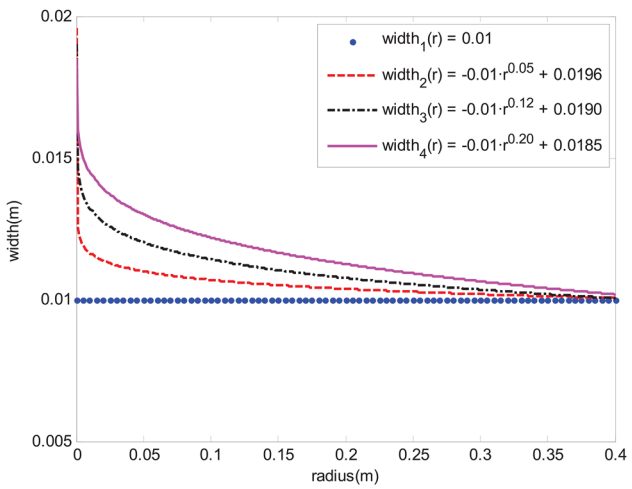

Fig. 5 The plot width *w* versus radius *r* for four representative width distribution function

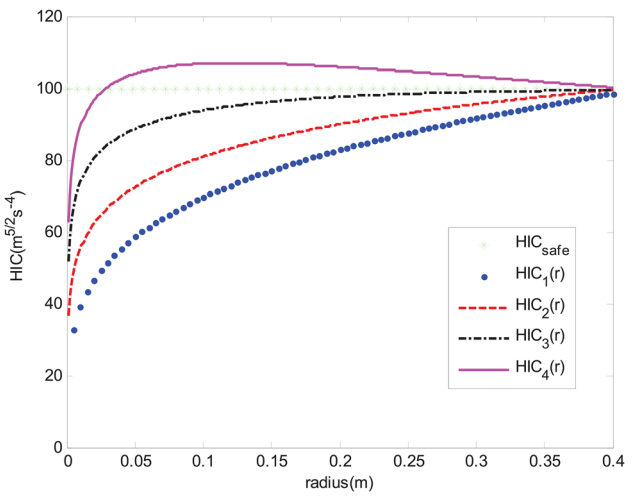

Fig. 6 The plot HIC as a function of radius *r* for the four width distribution functions given in Fig. 4

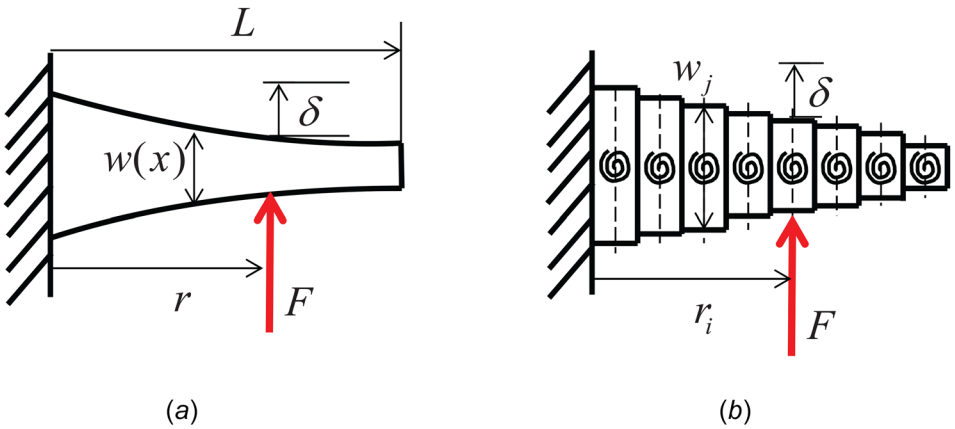

(a) (b)

Fig. 7 The continuous link model versus the discrete rigid segment model

Now our goal is to find the optimal width distribution function $w(x)$ such that the HIC distribution $\mathrm{HIC}(x)$ is as close to a given constant safety threshold $\mathrm{HIC}_{\mathrm{safe}}$ as possible. Therefore, our shape optimization problem can be written as

$$\min_{w(x)} \int_0^L \|\mathrm{HIC}_{\mathrm{safe}} - \mathrm{HIC}(x)\| dx \tag{4}$$

where the typical value of $\mathrm{HIC}_{\mathrm{safe}}$ is 100.

Since the width distribution $w(x)$ is unknown, it is not convenient to calculate the integration in Eq. (3). Let us discretize the link into n rigid segments joined with n torsion springs, as shown in Fig. 7(*b*). Now the effective stiffness in Eq. (3) can be calculated as

$$k_{\mathrm{eff}}(r_i) = \frac{1}{\sum_{j=1}^{i} \dfrac{12(r_i - r_j)^2}{E t w_j^3} \Delta r}, \quad 1 \le i \le n \tag{5}$$

where w_j is the link width at $x = r_j$, $\Delta r = L/n$ is the length of each segment. Now the HIC distribution function can be calculated as a function of r_i, i.e., $\mathrm{HIC}(r_i)$.

Now the shape optimization in Eq. (4) can be turned into the following n dimensional optimization problem:

$$\min_{w_i} \sum_{i=1}^{n} \|\mathrm{HIC}_{\mathrm{safe}} - \mathrm{HIC}(r_i)\| \tag{6}$$

Based upon the model established above, a program is designed to find the optimized width. The link is discretized into n segments in the beginning. For each segment, an initial width is provided to start to explore the optimized one to guarantee the corresponding HIC value approaches to the desired one. The exploring process is repeated with new width input until the absolute error between the actual HIC value and the desired one is less than a threshold. The new width value is updated with a fixed step length h which

Table 1 Shape optimization parameters and results

Angular velocity	$\omega = 0.8$ rad/s
Thickness	$t = 0.05$ m
Length	$L = 0.4$ m
Initial width	$w_0 = 0.015$ m
Young's modulus	$E = 200$ GPa
Mass of operator's head	$m_{\mathrm{oper}} = 4$ kg
Density of link's material	$\rho = 7900\,\mathrm{kg/m^3}$
Segment count	$n = 1000$
Error threshold of HIC	$e = 0.005\ \mathrm{m^{5/2}\ s^{-4}}$
Fixed step length of width	$h = 0.0001$ m
Desired HIC value	$\mathrm{HIC}_{\mathrm{safe}} = 100\ \mathrm{m^{5/2}\ s^{-4}}$
Optimal HIC value	$\mathrm{HIC}_V = 100 \pm 0.005\ \mathrm{m^{5/2}\ s^{-4}}$

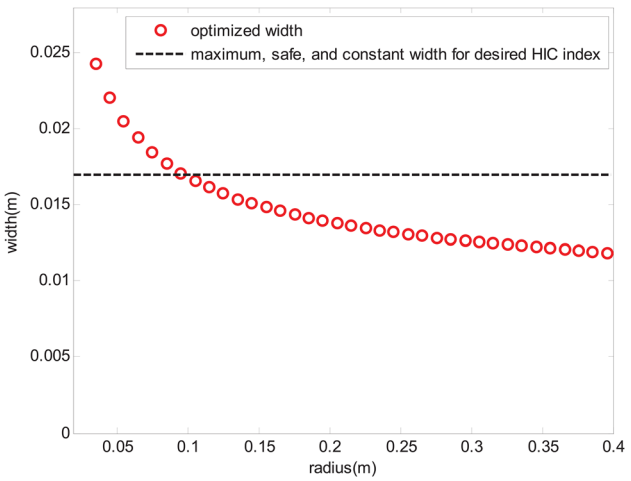

Fig. 8 The optimized width distribution of the link

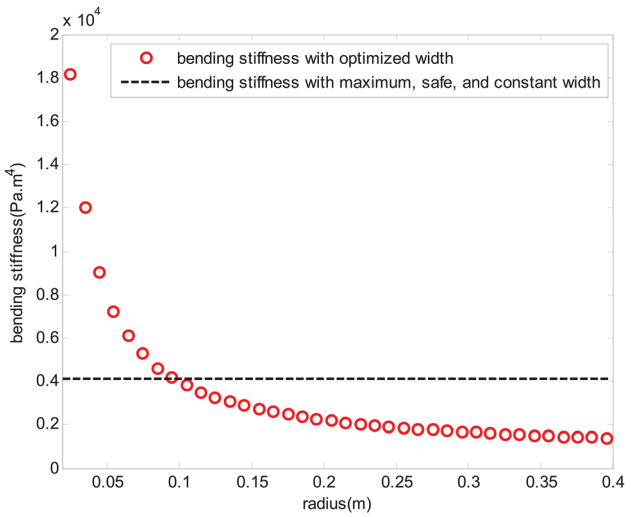

Fig. 9 The optimized bending stiffness *EI*

enables the real HIC value to gradually converge to the safe HIC value.

4.2 Optimization Results. Applying the optimization algorithm described earlier, we obtain the optimized width distribution of the link, which makes the actual HIC value close enough to the desired HIC value. The input parameters and the output results are shown in Table 1.

With these parameters, one can find the optimized width of the link with a variable width, shown as the circle line in Fig. 8. In contrast, if the link is with a uniform width, to ensure that the robot is safe (HIC $\leq$ 100 $m^{5/2}$ s^{-4}), the maximum safe width is 0.017 m, as shown as the dashed line in Fig. 8.

The optimized bending stiffness is shown in Fig. 9. The circle line is the optimized bending stiffness, while the dashed line is the *EI* value based upon a constant width of 0.017 m. It is obvious that the *EI* value for the uniform width link is a constant, while the *EI* value decreases along the radius of the link with the optimized width. The latter is a compliant link with a larger stiffness at the bottom and a smaller stiffness at the tip.

The optimized HIC distribution is shown as the circle line in Fig. 10, while the dashed line shows the HIC index with a constant width of 0.017 m. The optimized HIC is almost a constant and very close to 100 $m^{5/2}$ s^{-4} (error $\leq 5 \times 10^{-5}$%). The solution always converge to 100 ± 0.005 $m^{5/2}$ s^{-4} with different initial width values. The discretized number of the link n and the exploring step length of width h are the major factors to determine consumed time of operation. The more segments discretized, the more time consumed. Also, the smaller step length, the more time needed for computing. In this case, for the condition of $n = 1000$ and $h = 0.0001$ m, it took 0.835 s in MATLAB for the whole calculation.

4.3 Verification Via Human–Robot Impact Simulations. To demonstrate the optimized algorithm, the variable width link is modeled using MATLAB's Simmechanics toolbox, as shown in Fig. 11. The link is comprised of 101 segments connected by 100 torsion springs (k_l), and the load and operator are connected by a covering spring (k_c). An acceleration sensor is placed on the prismatic joint of the operator, which is able to provide acceleration for HIC calculation. The optimized widths calculated from MATLAB are exported to the Simmechanics model for verification, while other parameters of the model are defined in Simmechanics according to dimensions and properties of the link. After the simulation is done, the HIC value is output to the workspace of the MATLAB.

The basic idea is to compare the HIC value between the results from MATLAB calculation and from Simmechanics. Parameters of the impact system are the same as given in Sec. 4.2. On one hand, one can calculate acceleration based upon on expressions in Ref. [15] multiplying a constant factor of 9.8 m/s^2. On the other hand, one can obtain acceleration from Simmechanics. In this study, we obtained the HIC value from MATLAB calculation was 100.05 $m^{5/2}$ s^{-4}, while 98.75 $m^{5/2}$ s^{-4} from Simmechanics, with an error of 1.3%. The simulation verified the optimization frame of the variable width link.

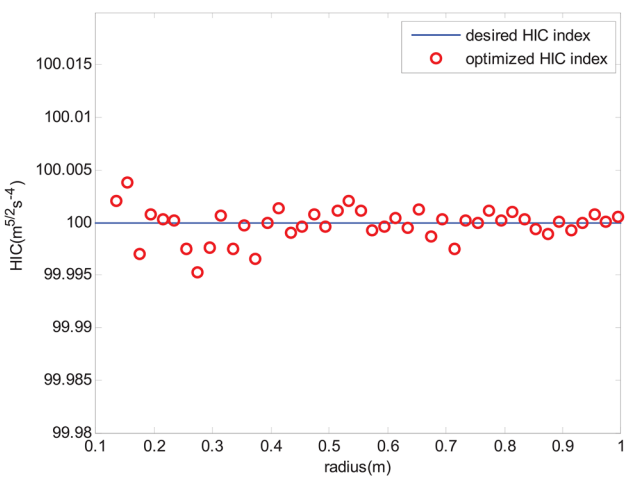

Fig. 10 The optimized HIC distribution along the link direction

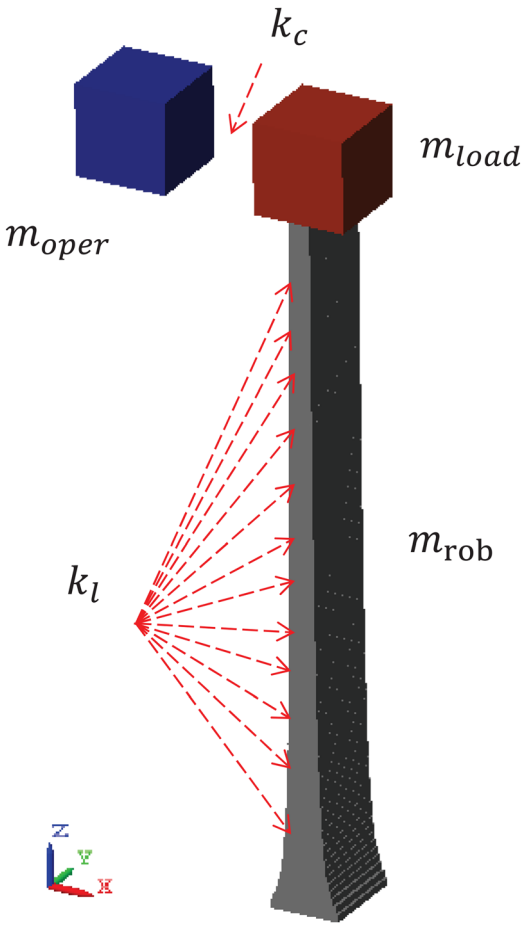

Fig. 11 The Simmechanics model for impact simulation

5 Modeling of the Variable Width Arm

After completing the design and optimization of the variable width arm, in this section, we would like to model the link from the perspective of statics and kinematics. We will model the

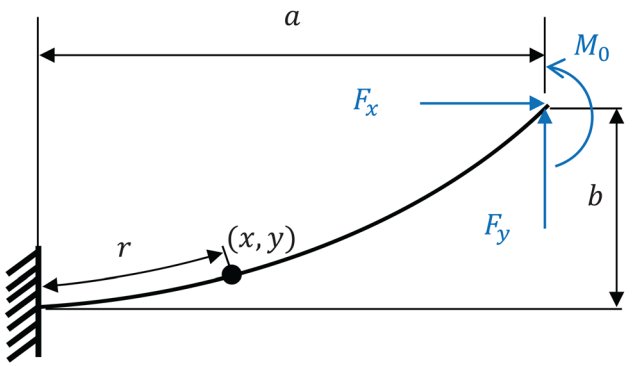

Fig. 12 The static model of the variable width link

variable width link using both the beam equation, which will be verified by ABAQUS finite element analysis (FEA).

From the optimization framework, we have obtained the shape of the inherently safe arm, which can be represented as a power equation of $w(r) = pr^q$, where p and q are width constants. Then, one can derive the static model of the variable width link using Bernoulli–Euler equation. Assume that a lateral impact force is applied on the tip of the link, generating the deformation of the link as shown in Fig. 12. As a general case, assume F_y, F_y, and M_0 are applied at tip of the link causing a tip deflection of $(L-a)$ and b in the x and y direction, respectively.

Any point away from the base of r comply with the Bernoulli–Euler beam equation

$$EI(r)\theta'(r) = M(r) \tag{7}$$

where

$$M(r) = M_0 + F_y(a - x(r)) - F_x(b - y(r))$$
$$I(r) = \frac{1}{12}tp^3r^{3q}$$

Take derivative of Eq. (7) and consider $dx/dr = \cos\theta$ and $dy/dr = \sin\theta$, the static model of the variable width link can be stated as follows:

$$EI(r)\theta''(r) + EI'(r)\theta'(r) = F_x \sin\theta - F_y \cos\theta \tag{8}$$

Since the impact force mostly occurs in the lateral direction, the initial conditions can be assigned as $\theta(0) = 0, \theta'(l) = 0$. From the optimization results we obtained, $p = 0.0079, q = -0.3492$. With these parameters we solve Eq. (8) and obtain the static and kinematics model of the variable width link.

To verify the derived static model, we build the variable width link model in ABAQUS FEA and compare their results. The tip locus are as shown in Fig. 13. The parameters of the link is from the optimization results. The lateral force is given as 1.35 kN. It is observed that the result of static model is very close to that of the FEA model, even under a very large deformation of $\delta/L = 62\%$.

6 Performance Evaluation

After finalizing the design and modeling of the variable width link of Fig. 4(*d*), we now evaluate its performance by comparing with other designs, such as those in Figs. 4(*b*) and 4(*c*). The compliant link with variable width and rigid joint, the compliant link with uniform width and rigid joint, and the rigid link with compliant joint, and the rigid link with rigid joint are subscripted with U, V, CJ, and RL for convenient analysis. The parameters in the following simulations refer those from the design stage, if not specified. In this section, their performances from perspectives of control, mechanical, and safety are compared and analyzed.

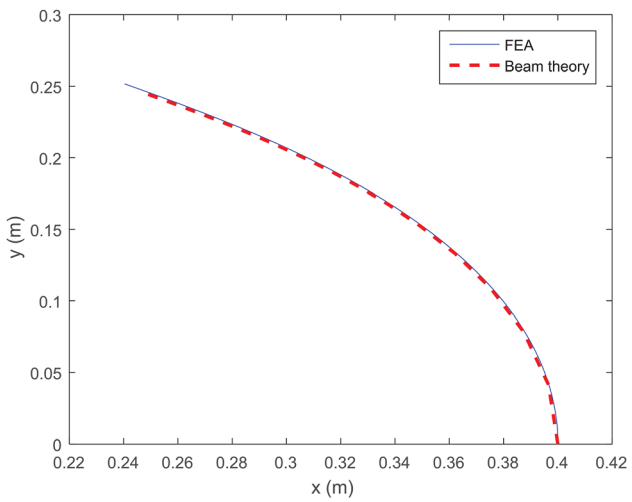

Fig. 13 Trajectory of the deflected tip point according to the FEA simulation and static model

6.1 Evaluation of the Natural Frequency. The natural frequency of the vibration system is one of the most important characteristics for dynamic analysis. The fundamental frequency is the dominant frequency in bending vibrations in many cases. A higher fundamental frequency may permit a larger bandwidth, even though they may not subject to analytical relations considering the high degree-of-freedom of the compliant links.

The compliant link with variable width, the compliant link with uniform width, and the rigid link with rigid joint are modeled in ABAQUS FEA, from which their fundamental natural frequency of f_U, f_V, and f_{RL} can be obtained, as shown in Table 2. The fundamental frequency of the rigid link with compliant joint, f_{CJ}, can be calculated according to its dynamics equation.

Since damping of the system does not affect the natural frequency, we can ignore the velocity term, and the dynamics of the compliant joint design can be described as

$$m_{CJ}\ddot{\theta} + k_{CJ}\theta = \tau \tag{9}$$

where the inertia matrix m_{CJ} and stiffness matrix k_{CJ} are calculated as follows:

$$m_{CJ} = \left(\frac{1}{3}m_{rob} + m_{load}\right)L^2, \quad k_{CJ} = \frac{3EI}{L}$$

The stiffness matrix k_{CJ} is calculated in such a way so that its lateral stiffness is equivalent to that of the compliant links. The natural frequency of the compliant joint design can be represented in the following form:

$$f_{CJ} = \frac{1}{2\pi}\sqrt{\frac{k_{CJ}}{m_{CJ}}} \tag{10}$$

The result is f_{CJ} as shown in Table 2. It is observed that the fundamental frequency of these systems has the following relations: $f_{CJ} < f_U < f_V < f_{RL}$. It is not surprised that the rigid link design has the highest fundamental frequency. Comparing the compliant designs (f_{CJ}, f_U, and f_V), it is observed that the variable width link has the highest fundamental frequency, and the compliant joint design has the lowest one among the three. It is well known that robots mostly work with a low frequency, and their input signal usually needs to avoid the resonance frequency. A design with a higher natural frequency may permit the input signal to have a wider range of operation frequency.

6.2 Evaluation of the Bandwidth. The bandwidth of a linear system has an analytical expression considering the first- and second-order systems. However, the compliant links have infinite degrees-of-freedom and do not follow the rule. To analysis their bandwidth, we model the four systems in Adams. Given a sinusoidal input of the joint angle, we measure the displacement response at the tip of the link. At a steady-state of vibration, the bandwidth can be specified when the normalized output signal decays a factor of 0.707.

The first step is to estimate the approximate range of the bandwidth of the four systems. Take the compliant link with a uniform

Table 2 Natural frequency of the four systems (Hz)

Mode	f_{CJ}	f_U	f_V	f_{RL}
1	37.219	43.107	103.24	$+\infty$

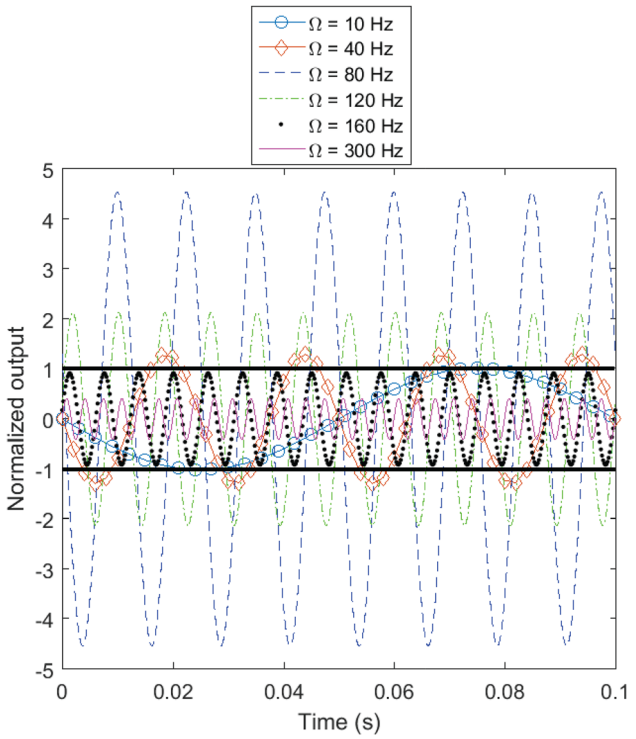

Fig. 14 Normalized displacement at the tip of the link given sinusoidal input signal at the joint angle

width as an example, the sinusoidal function with a wide range of frequencies (Ω) is given as the input signal, and the output response is chosen from the tip displacement of the compliant link, which is normalized for convenient analysis. The tip displacement has a large vibration in the beginning of the simulation, and gradually decays and finally reaches a stabilized state as shown in Fig. 14. Given a low frequency of the input signal such as $\Omega = 10$ Hz, the output response has no decays. As the increase of Ω, the magnitude of the output oscillation increase first then decreases later. The maximum magnitude may occurs at which the frequency of the input signal is close to the fundamental frequency and the resonance occurs. After the fundamental

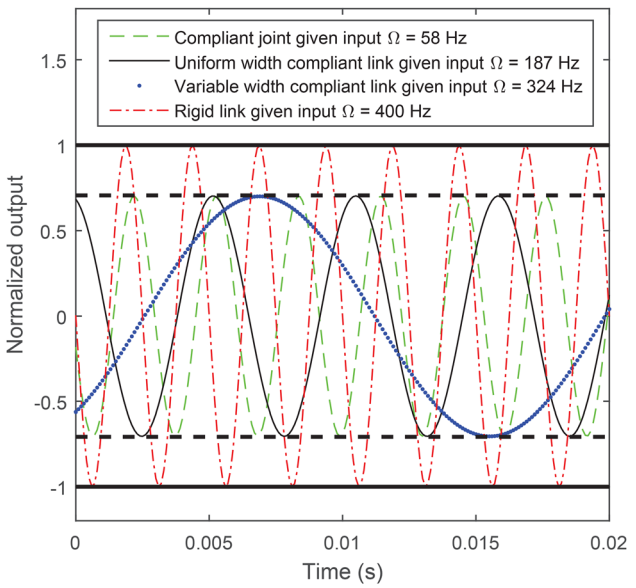

Fig. 15 Compare the bandwidth of the four systems

Table 3 Bandwidth of the four systems (Hz)

Bandwidth	W_{CJ}	W_U	W_V	W_{RL}
Value	58	187	324	$+\infty$

frequency, the higher frequency of the input signal results in larger decays of the output response during the stabilized state. Based on Fig. 14, one may claim that the bandwidth of the uniform width link may be between 160 Hz and 300 Hz according to this figure. The same procedures applied to the other three links to estimate the rough range of their bandwidth.

The second step is to specify the critical value of the bandwidth. Followed by the estimation of the rough range of the bandwidth, more frequency values are tried in Adams until an input frequency leads to the normalized output with a decay of 0.707. Their stabilized displacement responses are as shown in Fig. 15. The normalized output of the compliant joint design decays with 0.707 at $\Omega = 58$ Hz, while 0.707 decayed frequency of uniform width compliant link and variable width compliant link are $\Omega = 187$ Hz and $\Omega = 324$ Hz, respectively. The output of the rigid link has no decays no matter how larger the input frequency is given, and Fig. 15 shows an example of the output response given $\Omega = 400$ Hz. Therefore, we claim that the bandwidth of the fours systems are as shown in Table 3. It is observed that among the compliant designs, the variable width compliant link has the largest bandwidth, while the compliant joint design has the lowest bandwidth. Generally speaking, a higher bandwidth admits a quicker time response with a smaller settling time. Since the proposed compliant link has the largest bandwidth, it may permit the quickest response among the three compliant designs.

6.3 Evaluation of Stress Distribution. From the viewpoint of mechanical, we would like to explore the maximum stress distribution along the link. The stress of the link could be calculated by

$$\sigma(r) = \frac{M(r)y}{I(r)} \tag{11}$$

where

$$M(r) = EI(r)\theta'(r)$$

y is the distance away from the neutral plane at each cross section. The maximum stress at any cross section will occur on the outside

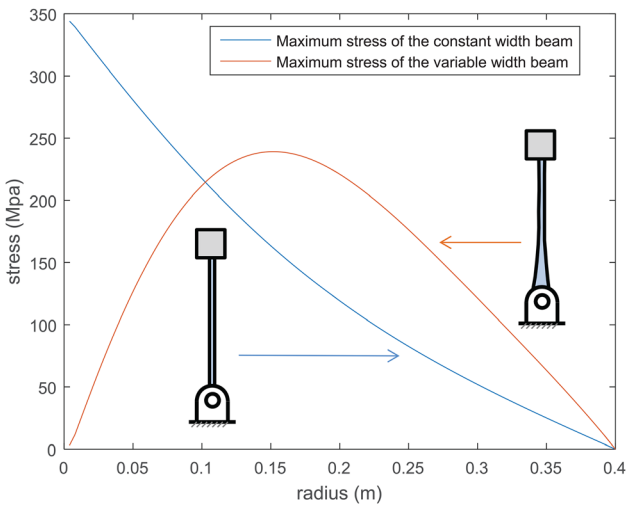

Fig. 16 Stress evaluation

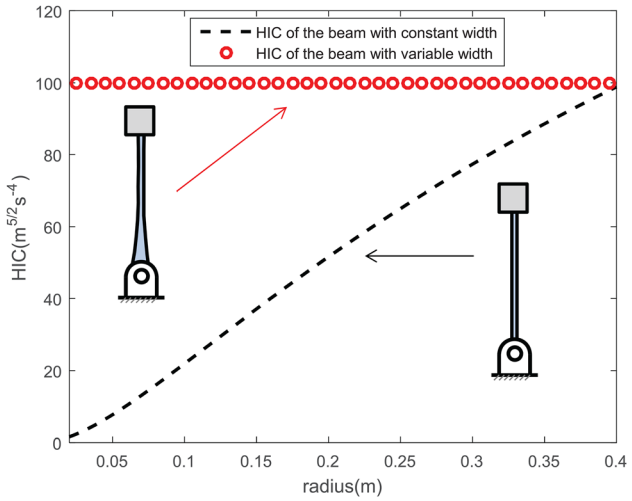

Fig. 17 Safety evaluation

surface link, i.e., $y = t/2$. The stress distribution of the uniform width link can be calculated according to Eq. (11) by holding the width as a constant value, while the stress of the variable width can be achieved given the width function. In this simulation, 1.35 kN lateral force is applied. The maximum stress distribution of the uniform width link and variable width link are as shown in Fig. 16. The stress on the link of Figs. 4(*a*) and 4(*d*) are 0 since they are regarded as rigid link and have no strain. It is observed that the stress on the uniform width link is nearly linearly distributed and has a high value at the base of the link, while the stress on the variable width is more gently distributed. The peak value of stress of the variable width is less than that of the uniform width. The stress distribution shows that the variable width link utilizes the mechanical compliance better than that of the uniform width link, and protect the robotic link better.

It is well known that robots mostly work at a low frequency. To avoid resonance vibration during a typical operation, it is better for the robot to have a high natural frequency or high bandwidth such that it provides a wider range of frequency of the input signal. In addition, it is generally true that a higher bandwidth admits a quicker response with a smaller settling time. Since the proposed compliant link is proved with a larger natural frequency/bandwidth than those of the compliant joint, the compliant link has the advantages with respect to the range of operation frequency and response time.

6.4 Evaluation of Safety. From the perspective of safety, the variable width link could obtain a uniform HIC distribution which is under a safety threshold. In contrast, the uniform width link has a gradually increase HIC value along the radial direction, as shown in Fig. 17. The HIC value increases from a small value to 100 $m^{5/2}$ s^{-4} at $r = 0.4$ m.

From the optimized results, one obtains the mass of the discrete beam with a variable width of 8.720 kg, while the mass of the continuous beam with a uniform width is 8.724 kg. The effective stiffness of the discrete beam with a variable width is 1.999×10^5 N/m, while the effective stiffness of the continuous beam with a uniform width is 1.989×10^5 N/m. The results show that both the mass and effective stiffness between these two types of beam are very close, given a desired HIC threshold of 100 $m^{5/2}$ s^{-4}. It is worth noting that the robot mass, in addition to the stiffness, may significantly affect the robot performance. In this study, since the mass variation can be neglected, one can focus on studying the stiffness effect on the performance.

It is observed that both of the variable width link and the uniform width link are inherently safe. However, the link with a variable width makes full use of the area between the circled line and the dashed line in Fig. 17. The continuous width does provide inherently safe property under the same safety threshold for human–robot interaction, but its performance is compromised. The variable width link takes full advantage of the compliance but still keep inherently safe. The extra stiffness of the variable width acquired has brought better performance, such as the larger bandwidth and lower maximum stress.

7 Conclusions and Future Work

In this paper, lateral stiffness and HIC distribution for several designs of compliant links are analyzed and compared. An optimization framework as well as computational models are developed to determine the optimal link width for a desired HIC distribution along the link with inherently safety.

A static model of the variable width link are derived, which are verified by finite element simulations for large deflections. The optimized link presented in this paper takes full advantage of the mechanical compliance of the robotic link for improving the control performance (larger bandwidth and natural frequency) while satisfying the safety constraint. This paper demonstrates that the compliant link solution may be an alternative approach for addressing safety concerns of human–robot interactions. Future work include the study of design and control of robotic manipulators with two or more flexible links.

Acknowledgment

This material is based upon the work supported by the National Science Foundation.

Funding Data

- Directorate for Engineering (Grant No. CMMI-1637656).

Nomenclature

EI = bending stiffness of cross section
f_{CJ} = fundamental frequency of rigid links with compliant joints
f_{RL} = fundamental frequency of rigid links
f_U = fundamental frequency of uniform beams
f_V = fundamental frequency of variable stiffness beams
HIC = head injury criterion
k_{CJ} = stiffness of rigid links with compliant joints
m_{CJ} = inertia of rigid links with compliant joints
W_{CJ} = bandwidth of rigid links with compliant joints
W_{RL} = bandwidth of rigid links
W_U = bandwidth of uniform beams
W_V = bandwidth of variable stiffness beams

References

[1] Edward Colgate, J., Wannasuphoprasit, W., and Peshkin, M. A., 1996, "Cobots: Robots for Collaboration With Human Operators," International Mechanical Engineering Congress and Exhibition, Atlanta, GA, Nov. 17–22, pp. 433–439.
[2] Chu, A., Kazerooni, H., and Zoss, A., 2005, "On the Biomimetic Design of the Berkeley Lower Extremity Exoskeleton (BLEEX)," IEEE International Conference on Robotics and Automation (ICRA), Barcelona, Spain, Apr. 18–22, pp. 4345–4352.
[3] Frisoli, A., Rocchi, F., Marcheschi, S., Dettori, A., Salsedo, F., and Bergamasco, M., 2005, "A New Force-Feedback Arm Exoskeleton for Haptic Interaction in Virtual Environments," First Joint Eurohaptics Conference, Symposium on Haptic Interfaces for Virtual Environment and Teleoperator Systems, World Haptics (WHC), Pisa, Italy, Mar. 18–20, pp. 195–201.
[4] Roderick, S., and Carignan, C., 2007, "Designing Safety-Critical Rehabilitation Robots," *Rehabilitation Robotics*, S. S. Kommu, ed., InTech, Vienna, Austria.
[5] Wolbrecht, E., Chan, V., Reinkensmeyer, D., and Bobrow, J., 2008, "Optimizing Compliant, Model-Based Robotic Assistance to Promote Neurorehabilitation," IEEE Trans. Neural Syst. Rehabil. Eng., **16**(3), pp. 286–297.
[6] Bicchi, A., and Tonietti, G., 2004, "Fast and 'Soft-Arm' Tactics [Robot Arm Design]," IEEE Rob. Autom. Mag., **11**(2), pp. 22–33.
[7] Bicchi, A., Tonietti, G., and Piaggio, E., 2002, "Design, Realization and Control of Soft Robot Arms for Intrinsically Safe Interaction With Humans," IARP/RAS Workshop on Technical Challenges for Dependable Robots in Human Environments, Toulouse, France, Oct. 7–8, pp. 79–87.

[8] ISO, 1992, "Robots for Industrial Environments—Safety Requirements. Part I: Robot," International Organization for Standardization, Geneva, Switzerland, Standard No. ISO 10218:1992.
[9] ISO, 2006, "Robots for Industrial Environments—Safety Requirements. Part I: Robot," International Organization for Standardization, Geneva, Switzerland, Standard No. ISO 10218-1:2006.
[10] Versace, J., 1971, "A Review of the Severity Index," SAE Paper No. 710881.
[11] Newman, J. A., Shewchenko, N., and Welbourne, E., 2000, "A Proposed New Biomechanical Head Injury Assessment Function—The Maximum Power Index," Stapp Car Crash J., **44**, pp. 215–247.
[12] Gadd, C. W., 1966, "Use of a Weighted-Impulse Criterion for Estimating Injury Hazard," SAE Paper No. 660793.
[13] Newman, J. A., 1980, "Head Injury Criteria in Automotive Crash Testing," SAE Paper No. 801317.
[14] Pervez, A., and Ryu, J., 2008, "Safe Physical Human Robot Interaction-Past, Present and Future," J. Mech. Sci. Technol., **22**(3), pp. 469–483.
[15] Gao, D., and Wampler, C. W., 2009, "Head Injury Criterion," IEEE Rob. Autom. Mag., **16**(4), pp. 71–74.
[16] Haddadin, S., Albu-Schäffer, A., and Hirzinger, G., 2009, "Requirements for Safe Robots: Measurements, Analysis and New Insights," Int. J. Rob. Res., **28**(11–12), pp. 1507–1527.
[17] Zheng, Y.-F., and Hemami, H., 1985, "Mathematical Modeling of a Robot Collision With Its Environment," J. Rob. Syst., **2**(3), pp. 289–307.
[18] Howe, R. D., and Cutkosky, M. R., 1993, "Dynamic Tactile Sensing: Perception of Fine Surface Features With Stress Rate Sensing," IEEE Trans. Rob. Autom., **9**(2), pp. 140–151.
[19] Feddema, J. T., and Novak, J. L., 1994, "Whole Arm Obstacle Avoidance for Teleoperated Robots," IEEE International Conference on Robotics and Automation (ICRA), San Diego, CA, May 8–13, pp. 3303–3309.
[20] Lumelsky, V. J., and Cheung, E., 1993, "Real-Time Collision Avoidance in Teleoperated Whole-Sensitive Robot Arm Manipulators," IEEE Trans. Syst., Man Cybern., **23**(1), pp. 194–203.
[21] Heinzmann, J., and Zelinsky, A., 2003, "Quantitative Safety Guarantees for Physical Human-Robot Interaction," Int. J. Rob. Res., **22**(7–8), pp. 479–504.
[22] Kong, K., Bae, J., and Tomizuka, M., 2009, "Control of Rotary Series Elastic Actuator for Ideal Force-Mode Actuation in Human–Robot Interaction Applications," IEEE/ASME Trans. Mechatronics, **14**(1), pp. 105–118.
[23] Najmaei, N., and Kermani, M. R., 2011, "Applications of Artificial Intelligence in Safe Human–Robot Interactions," IEEE Trans. Syst., Man, Cybern., Part B: Cybern., **41**(2), pp. 448–459.
[24] Avanzini, G. B., Ceriani, N. M., Zanchettin, A. M., Rocco, P., and Bascetta, L., 2014, "Safety Control of Industrial Robots Based on a Distributed Distance Sensor," IEEE Trans. Control Syst. Technol., **22**(6), pp. 2127–2140.
[25] Zinn, M., Khatib, O., and Roth, B., 2004, "A New Actuation Approach for Human Friendly Robot Design," IEEE International Conference on Robotics and Automation (ICRA), New Orleans, LA, Apr. 26–May 1, pp. 249–254.
[26] Tonietti, G., Schiavi, R., and Bicchi, A., 2006, "Optimal Mechanical/Control Design for Safe and Fast Robotics," *Experimental Robotics IX*, Springer, Berlin, pp. 311–320.
[27] Bicchi, A., Bavaro, M., Boccadamo, G., De Carli, D., Filippini, R., Grioli, G., Piccigallo, M., Rosi, A., Schiavi, R., Sen, S., and Tonietti, G., 2008, "Physical Human-Robot Interaction: Dependability, Safety, and Performance," Tenth IEEE International Workshop on Advanced Motion Control (AMC), Trento, Italy, Mar. 26–28, pp. 9–14.
[28] Chen, L., Garabini, M., Laffranchi, M., Kashiri, N., Tsagarakis, N. G., Bicchi, A., and Caldwell, D. G., 2013, "Optimal Control for Maximizing Velocity of the CompAct^{TM} Compliant Actuator," IEEE International Conference on Robotics and Automation (ICRA), Karlsruhe, Germany, May 6–10, pp. 516–522.
[29] Haddadin, S., Albu-Schaffer, A., Eiberger, O., and Hirzinger, G., 2010, "New Insights Concerning Intrinsic Joint Elasticity for Safety," 2010 IEEE/RSJ International Conference on Intelligent Robots and Systems (IROS), Taipei, Taiwan, Oct. 18–22, pp. 2181–2187.
[30] Lim, H.-O., and Tanie, K., 2000, "Human Safety Mechanisms of Human-Friendly Robots: Passive Viscoelastic Trunk and Passively Movable Base," Int. J. Rob. Res., **19**(4), pp. 307–335.
[31] She, Y., Meng, D., Cui, J., and Su, H.-J., 2017, "On the Impact Force of Human-Robot Interaction: Joint Compliance vs. Link Compliance," IEEE International Conference on Robotics and Automation (ICRA), Singapore, May 29–June 3, pp. 6718–6723.
[32] Stilli, A., Grattarola, L., Feldmann, H., Wurdemann, H. A., and Althoefer, K., 2017, "Variable Stiffness Link (Vsl): Toward Inherently Safe Robotic Manipulators," IEEE International Conference on Robotics and Automation (ICRA), Singapore, May 29–June 3, pp. 4971–4976.
[33] She, Y., Su, H.-J., Lai, C., and Meng, D., 2016, "Design and Prototype of a Tunable Stiffness Arm for Safe Human-Robot Interaction," ASME Paper No. IDETC2016-59523.
[34] She, Y., Su, H.-J., and Hurd, C. J., 2015, "Shape Optimization of 2D Compliant Links for Design of Inherently Safe Robots," ASME Paper No. DETC2015-46622.
[35] Ham, R., Sugar, T., Vanderborght, B., Hollander, K., and Lefeber, D., 2009, "Compliant Actuator Designs," IEEE Rob. Autom. Mag., **16**(3), pp. 81–94.